Hindawi Publishing Corporation
International Journal of Distributed Sensor Networks
Volume 2013, Article ID 125423, 9 pages
http://dx.doi.org/10.1155/2013/125423

Research Article

Circular Collaborative Beamforming for Improved Radiation Beampattern in WSN

N. N. Nik Abd Malik, M. Esa, S. K. Syed Yusof, S. A. Hamzah, and M. K. H. Ismail

UTM MIMOS CoE Telecommunication Technology, Faculty of Electrical Engineering, Universiti Teknologi Malaysia, 81310 Johor Bahru, Johor, Malaysia

Correspondence should be addressed to N. N. Nik Abd Malik; noordini@fke.utm.my

Received 1 March 2013; Revised 28 May 2013; Accepted 11 June 2013

Academic Editor: Adnan Kavak

This paper presents a novel collaborative beamforming (CB) method of wireless sensor network (WSN) by organizing sensor node location in a circular arrangement. Appropriate selection of active CB nodes and cluster is needed each time to perform CB. The nodes are modeled in circular array location in order to consider it as a circular antenna array (CAA). This newly proposed circular collaborative beamforming (CCB) is further presented to solve two different objectives, that is, sidelobe level (SLL) suppression and first null beamwidth (FNBW). Analyses obtained are compared to those from previous work. The findings demonstrate a better CB performance of intelligent capability, and the difference is shown in normalized power characteristic.

1. Introduction

Inside WSN environment, collaborative beamforming (CB) can be beneficial in increasing signal to noise ratio (SNR), thus boosting the energy efficiency of the system. In contrast with direct transmission transmitter-receiver or hop-by-hop transmission, CB spreads the energy consumption over multiple transmitters and improves the signal strength at the receiver [1]. Therefore, the CB nodes need less energy for data transmission, thus balance the energy consumptions, and desirably extend the network lifetime.

Works supporting sensor network in the literature, which utilizes wireless array, including [2–4] investigated usefulness of method and implementation schemes of a transmission array. Gaussian probability density function (pdf) is utilized to model the spatial distribution of sensor nodes in a cluster of WSNs [2] by proposing node selection algorithm [5]. The impact of Gaussian pdf as the spatial distribution is explored on the beampattern characteristic and compared with similar case when uniform pdf is used in [6]. The algorithm is developed to control the sidelobes by searching over different node combinations [7]. Ahmed and Vorobyov consider the random nodes deployed in Gaussian pdf, while the proposed work considers the uniform random nodes distribution.

In spite of the significant contributions from previous literatures on CB, none of the works offer a CB by implementing circular antenna array (CAA). To the best of the authors' knowledge, this is the first work dealing with this problem. In this paper, the circular array technique is specially designed for WSNs with intelligent capability. The conventional uniform circular antenna array (UCA) may not be directly applied in WSN as it requires the exact location of elements in circular arrangement, a requirement that does not conform with random distribution nature of sensor nodes. Therefore, this is the main challenge of adapting this CAA into the context of WSN environment.

This paper presents a novel method of optimizing sensor node location in a circular arrangement. In this problem, the appropriate selection of active CB nodes and cluster is needed at each time to perform CB in WSN. The nodes are modeled in circular array location in order to consider it as a CAA. In the preliminary version of this work [8], it is shown that the linear sensor nodes array (LSNA) is able to achieve a desirable adaptive beampattern with

narrow main lobe and acceptable sidelobes level (SLL). Novel concept is offered with regard to intelligently optimizing and locating the selected sensor nodes to participate and form an array of sensor nodes. The concept is extended here through an alternate approach which employs hybrid least-square speedy particle swarm optimization-based circular collaborative beamforming (HLPSO-based CCB). The earlier work is reported in [9]. The biologically-inspired algorithm of particle swarm optimization (PSO) algorithm is improved and utilized to select the optimum nodes to participate in CB. The objective is to keep the main advantages of the standard PSO, such as simple implementation, low algorithmic complexity, and few control parameters, while maintaining the performance. Therefore, the proposed HLPSO characteristics are particularly attractive for WSNs since the computational resources such as memory and energy are limited.

The main idea in the proposed method is the desired objectives of radiation beampattern with minimum SLL and controllable size of FNBW The proposed intelligent method of HLPSO-based CCB for determining optimum location of sensor node is proved superior to alternate techniques in terms of the normalized power gain with desired objectives. Up to date, an intelligent approach to determine optimum sensor nodes location to participate in wireless array network by employing bioinspired algorithm has not been reported or published so far by other authors.

2. The Network and Geometrical Array Model

2.1. The Network Model. WSN consists of a large number of sensor nodes in random deployment, which are wirelessly connected. The nodes are self-organized and are in connection with a controlling station as described in [10]. Each sensor node's location is determined using location discovery techniques [11] and is reported back to the controller. The central processor in a controlling station has detailed knowledge of each sensor node's location. It is also capable of selecting the appropriate manager node (MN), thus active cluster (AC) as per user requirement. Each sensing node, S_z is able to sense the environment and collect its own data. The selected MN gathers the data from the sensing nodes and then multicasts a final data packet to all the selected collaborative sensor nodes, that is, active CB nodes. The data from these sensing nodes are aggregated at the MN and only the needed information will be multicast. The active CB nodes will collaboratively transmit the same data in a synchronous manner. These active CB nodes, which perform as a CAA, have the possibility to form a narrow highly directive beam to the intended target point, where the receivers may be placed in order to collect all the transmitted data sent by collaborative nodes.

2.2. The Geometrical Array Model. The collaborative array antenna radiates power in all directions; hence, the simulation work should be in 3-dimensional scope. It is assumed that all sensor nodes are located on a 3-dimensional x-y-z plane. Consider a 3-dimensional characteristic of N-element CAA placed at the x-y-z plane. Assume $z = 0$; therefore the plane is visualized to run parallel to the earth's surface. The array factor (AF) of the CAA [12] is given by

$$\begin{aligned} \mathrm{AF}(\theta,\phi) &= \sum_{n=1}^{N} e^{j[\kappa r_n \sin\theta\cos(\phi-\phi_n)+\alpha_n]}, \\ \alpha_n &= -\kappa r_n \sin\theta_0 \cos(\phi_0 - \phi_n), \\ r_n &= \sqrt{(x_n)^2 + (y_n)^2}, \\ \phi_n &= \tan^{-1}\left(\frac{y_n}{x_n}\right), \end{aligned} \tag{1}$$

where N, κ, θ, ϕ, x_n, and y_n are the number of elements, wavenumber $\kappa = 2\pi/\lambda$, elevation angle, azimuth angle, x-coordinate, and y-coordinate (x_n, y_n) of the nth element, respectively. θ_0 and ϕ_0 are the maximum radiation angles. The normalized power gain, G_{norm}, in decibel is as stated in

$$G_{\mathrm{norm}}(\theta,\phi)_{\mathrm{dB}} = 10\log_{10}\left[\frac{|\mathrm{AF}(\theta,\phi)|^2}{\max|\mathrm{AF}(\theta,\phi)|^2}\right]. \tag{2}$$

3. Hybrid Least-Square Speedy Particle Swarm Optimization (HLPSO)

PSO is applied to determine the optimum distance location of the nodes, which performs the highest performance as refer to objective scopes. Some improvements have been adopted in original PSO [13] in order to overcome the weaknesses and to adapt the algorithm inside WSNs environment. The novel HLPSO is proposed by integrating two novel mechanisms, that is, constraint boundaries variables and particle's position and velocity reinitialization. Moreover, the least-square approximation algorithm (LS) is integrated into it to improve the effectiveness and the capabilities of PSO in CCB application.

3.1. Global Constraint Boundaries Variables. Two sets of global constraint boundaries variables for lower boundary L and upper boundary U for different position particles, d_{s1} and d_{sn} $(n = 2, 3, \ldots, N)$, are adopted and represented as

$$\begin{aligned} L_1 \le d_{s1} < U_1, \\ L_N \le d_{sn} < U_N. \end{aligned} \tag{3}$$

These two boundaries are applied to restrict d_{s1} and d_{sn} to stay inside the solution space. Additionally, maximum upper limit and minimum lower limit are also assimilated inside this proposed HLPSO, that is, $U_{\max}$ and $L_{\min}$, respectively. These two limits are determined before the computation of the objective function, of, in order to enhance the diversity

of the particle's searching abilities to be more global and freedom. Thus, it is expressed as

$$d_{s1} = \begin{cases} d_{s1} = L_1 \xrightarrow{\text{yields}} of\,(L_1), & \text{if } d_{s1} > U_{\max}, \\ d_{s1} = d_{s1} \xrightarrow{\text{yields}} of\,(d_{s1}), & \text{if } L_{\min} \le d_{s1} < U_{\max}, \\ d_{s1} = L_1 \xrightarrow{\text{yields}} of\,(L_1), & \text{if } d_{s1} \le L_{\min}, \end{cases}$$

$$d_{sn} = \begin{cases} d_{sn} = L_N \xrightarrow{\text{yields}} of\,(L_N), & \text{if } d_{sn} > U_{\max}, \\ d_{sn} = d_{sn} \xrightarrow{\text{yields}} of\,(d_{sn}), & \text{if } L_{\min} \le d_{sn} < U_{\max}, \\ d_{sn} = L_N \xrightarrow{\text{yields}} of\,(L_N), & \text{if } d_{sn} \le L_{\min}. \end{cases} \tag{4}$$

3.2. Particle's Position and Velocity Reinitialization. The random numbers of particle position d_{sn} can be a factor of the particle's tendency to leave the initially defined search space. Therefore, a modification based on the absorbing wall conditions by [14] is implemented in this algorithm. In order to control the movement of particle from flying outside the border of the search space, the velocity v_{sn} is zeroed whenever the particle d_{sn} goes over the boundaries U_N and L_N. However, the particle d_{sn} is then pulled back inside the search space by reinitializing it as random numbers r generated from the values of $[L_{\min}, U_{\max}]$. The objective of this reinitialization of d_{sn} is to prevent the particle from being stuck in local optima scenario where the particle is trapped and inhibited to search for a better solution. By introducing the reinitialization, a more flexible and comprehensive searching can be done by the particle with noted limitations, as expressed by

$$v_{sn} = \begin{cases} v_{sn} = 0 \longrightarrow d_{sn} = r\,[L_{\min}, U_{\max}], & \text{if } d_{sn} > U_N, \\ v_{sn} = v_{sn}, & \text{if } L_N \le d_{sn} < U_N, \\ v_{sn} = 0 \longrightarrow d_{sn} = r\,[L_{\min}, U_{\max}], & \text{if } d_{sn} \le L_N. \end{cases} \tag{5}$$

By using (5), the particle movement may be triggered again so that it has the highest probability to search for the optimum global best. In addition, the particle position is also forced to stay inside the upper boundary U and lower boundary L as denoted by following equations:

$$d_{s1} = \begin{cases} d_{s1} = U_1, & \text{if } d_{sn} > U_1, \\ d_{s1} = d_{s1}, & \text{if } L_1 \le d_{sn} < U_1, \\ d_{sn} = L_1, & \text{if } d_{sn} \le L_1, \end{cases}$$

$$d_{sn} = \begin{cases} d_{sn} = U_N, & \text{if } d_{sn} > U_N, \\ d_{sn} = d_{sn}, & \text{if } L_N \le d_{sn} < U_N, \\ d_{sn} = L_N, & \text{if } d_{sn} \le L_N. \end{cases} \tag{6}$$

The integration of the LS approximation algorithm in this HLPSO is required so that the desired radiation beampattern performance can be closely approximated to the desired beampattern results. Due to the random spatial positioning of nodes, LS algorithm provides the ability to alter and create a radiation beampattern by introducing weights on each node. The determination of the weights allows elimination of the effect of random nodes position errors in WSNs. The effect of weights can be removed through equalization.

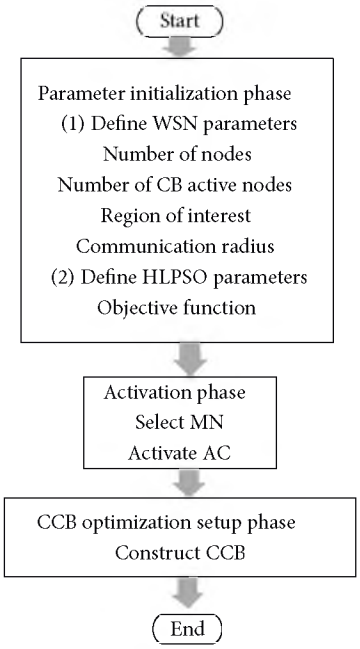

Figure 1: Flow chart for HLPSO-based CCB.

3.3. Hybrid Least-Square Particle Swarm Optimization-Based Circular Collaborative Beamforming (HLPSO-Based CCB). The proposed network model of HLPSO-based CCB consists of a random deployment of Z stationary sensor nodes inside the region of interest of $\Lambda\,\mathrm{m}^2$, which are organized in a different cluster. Each node is denoted in Cartesian coordinates of (x_k, y_k) with k representing the number of nodes. Each cluster has an MN designated as the leader, which manages in searching and selecting only the participating CB active nodes to form the HLPSO-based CCB in circular arrangement. The MN also acts as the centre of the CCB, but it is not participating in the CAA construction. Therefore, MN organizes a subset of its cluster nodes into a distributed CCB, $M_n = (m_1, m_2, \ldots, m_N)$ coordinating their transmissions to direct the main beam towards the receivers.

There are three phases in HLPSO-based CCB: parameter initialization, activation, and optimization setup phases. The flow chart for the three phases of HLPSO-based CCB has been shown in Figure 1. A description of each follows.

3.3.1. Parameter Initialization Phase. The initial parameters for WSNs environment are listed in Table 1.

The proposed HLPSO manages to search for the optimum element distance of CCB and deal with the desired objectives. The desired parameters for HLPSO are illustrated in Table 2. These parameters are initialized by referring to the desired objectives of the organization scheme.

Table 1: Parameters and values of 8-node CCB.

Parameters	Symbol	Values
Number of all nodes	Z	900 nodes
Area of interest	Λ	900 m^2
Density	ρ	1 node/m^2
Manager node	MN (x_{MN}, y_{MN})	(14.51, 20.91)
Area of active cluster	X	123 m^2
Nodes inside active cluster	Z_S	119
UCA radius	r^{UCA}	2.5464 m
CCB radius	r^{CCB}	2.9421 m

Table 2: List of parameters used in HLPSO implementation.

Parameters	Symbol	Value
Number of particles	S	30
Dimension of particles	N	8
Iterations	It	500–1000
Range of particles	D	0 to 2 λ_O
Upper boundary for d_n	U_N	2.2 λ_O
Lower boundary for d_n	L_N	0.1 λ_O
Maximum upper limit	U_{max}	0.1 λ_O
Maximum lower limit	L_{min}	2.5 λ_O
Velocity	V	0 to 0.2
Learning factors	$c_1 = c_2$	2.0
Maximum weight	ω_{max}	0.9
Minimum weight	ω_{min}	0.4

3.3.2. Activation Phase. MN with coordinates of (x_{MN}, y_{MN}) is activated which has the most neighbor nodes within its communication radius, C. Then, the AC area, Xm^2, is determined by referring to the MN as the centre of the X. The total number of nodes, Z_S, within X is activated.

3.3.3. CCB Optimization Setup Phase. The procedures needed to formulate this CCB optimization setup scheme are described as follows.

Step 1. Construct the virtual circle with C radius by referring to MN as the center of the circle.

Step 2. Establish HLPSO algorithm to optimize the sensor node location.

Step 2(a). Initialize HLPSO parameters.

Step 2(b). Generate random initial location, d_{sn}, $[d_{sn}] = [d_{s1}, d_{s2}, d_{s3}, \ldots, d_{sN}]$ and velocity, v_{sn}, $[v_{sn}] = [v_{s1}, v_{s2}, v_{s3}, \ldots, v_{sN}]$ for each particle, where N and s are the dimensional problem and number of particles, respectively.

Step 2(c). Calculate the objective function, that is, of, where of_{SLL} is the objective function of SLL minimization term as defined in

$$of_{SLL}(\theta_{SLL}) = \sum_{SLL_1=1}^{MaxSL} \left|AF(\theta_{SLL_1})\right|_{dB} + \sum_{MinSL}^{SLL_2=181} \left|AF(\theta_{SLL_2})\right|_{dB}, \quad (7)$$

where θ_{SLL_1} and θ_{SLL_2} are the angles, where the SLL is minimized in the lower band (from $\theta_{SLL_1=1}$ to $\theta_{SLL_1=MaxSL}$) and in the upper band (from $\theta_{SLL_2=MinSL}$ to $\theta_{SLL_2=181}$), respectively. of_{bw} is the objective function FNBW term as defined in

$$of_{bw}(\theta_{bw}) = \sum_{bw=bw1}^{bw2} \left|AF(\theta_{bw})\right|_{dB}, \quad (8)$$

where θ_{bw} is the angle of desired FNBW; that is, FNBW = $\theta_{bw2} - \theta_{bw1}$ which is the range of angles of the major lobe.

Step 2(d). Determine the previous best location, *pbest*, $P = [p_s] = [p_1, p_2, p_3, \ldots, p_S]$. Set $of(p_s)$ value to be equal to $of(d_{sn})$.

Step 2(e). Determine the global best position, $G = [g_n] = [g_1, g_2, g_3, \ldots, g_N]$. Set $g_n = \min(p_s)$ or $g_n = \text{optimum}(p_s)$.

Step 2(f). Update v_{sn}:

$$v_{sn}(\tau+1) = \omega v_{sn}(\tau) + c_1 r_1 [p_s(\tau+1) - x_{sn}(\tau)] + c_2 r_2 [g_n(\tau+1) - x_{sn}(\tau)], \quad (9)$$

where c_1 and c_2 are acceleration constants and r_1 and r_2 are uniformly distributed numbers in $[0, 1]$. $\tau + 1$ and τ refer to the time index of the current and previous iterations. ω is the inertial weight factor. Then, limit V using (5).

Step 2(g). Update d_{sn}:

$$d_{sn}(\tau+1) = d_{sn}(\tau) + v_{sn}(\tau+1) \quad (10)$$

and limit D of the particles by using (6).

Step 2(h). Update *pbest* as follows.

If $of(d_{sn})$ is better than $of(p_s)$, then update p_s and store $d_{sn}(p_s)$.

Step 2(i). Update *gbest* as follows.

If $of(p_s)$ is better than $of(g_n)$, then update g_n and store $d_{sn}(g_n)$.

Step 2(j). If the maximum iteration number is met, terminate the algorithm, otherwise, proceed to Step 2(c).

Step 3. Construct CAA by using the distance result d_{sn} from the HLPSO algorithm. The constructed CAA is assumed with N-node with spacing distance of d_{sn}. The sensor node location of x- and y-coordinates, $B_n(x_n^B, y_n^B)$, is referring to the values of d_{sn}.

Step 3(a). Calculate the radius, r^d, from d_{sn} by using

$$r^d = \frac{\sum_{n=1}^{N} d_{sn}}{2\pi}. \quad (11)$$

Step 3(b). Calculate phase ϕ_n for every d_{sn} $(n = 1, 2, \ldots, N)$. These r^d and ϕ_n values are the polar coordinates of HLPSO optimized location of sensor nodes, $B_n(r^d, \phi_n)$. The ϕ_n is calculated using

$$\phi_n = \frac{\left(2\pi \sum_{n=1}^{N} d_{sn}\right)}{\sum_{n=1}^{N} d_{sn}}. \quad (12)$$

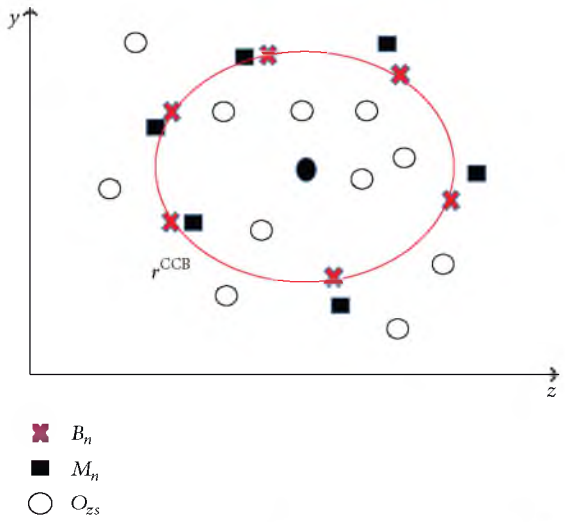

FIGURE 2: Locations of B_n, O_{zs}, and M_n with radius of r^{CCB}.

Step 3(c). Convert the polar coordinates $B_n(r^d, \phi_n)$, to the Cartesian coordinates, $B_n(x_n^B, y_n^B)$ by using

$$x_n^B = \left(r^d \cos\phi_n\right) + x_{\mathrm{MN}},$$
$$y_n^B = \left(r^d \sin\phi_n\right) + y_{\mathrm{MN}}, \tag{13}$$

where $(x_{\mathrm{MN}}, y_{\mathrm{MN}})$ are the coordinates of MN.

The construction of this optimum CAA is illustrated in Figure 2. The MN is located at the centre of B_n; however MN does not participate in this CAA. Virtual circle for B_n is constructed with a radius of r^{CCB}.

Step 3(d). Determine the normalized gain, G_{norm}^B, by using (2).

Step 4. Start searching CCB nodes.

Step 4(a). Select the minimum Euclidean distance, $d_n^{\min}$, between $B_n(x_n^B, y_n^B)$ and the nearest node inside AC, $O_{zs}(x_{zs}^O, y_{zs}^O)$,

$$\min\left\{\sqrt{\left[\left(x_n^B - x_{zs}^O\right)^2 + \left(y_n^B - y_{zs}^O\right)^2\right]}\right\} = d_n^{\min} \tag{14}$$

with $zs = 1, 2, \ldots, ZS$ nodes inside AC.

Step 4(b). Choose the O_{zs} which has $d_n^{\min}$ with coordinates (x_{zs}^O, y_{zs}^O)

Step 4(c). Activate O_{zs} and appoint it as an optimum CCB. CCB is represented as $M_n(x_n^M, y_n^M)$, $M_n \in O_{zs}$. The mapping process is illustrated in Figure 2.

Step 4(d). This set of optimal CCB will be performed collaboratively as an N-element distributed CAA.

Step 5. Determine normalized gain, $G_{\mathrm{norm}}^{\mathrm{CCB}}$, of final CCB using (2).

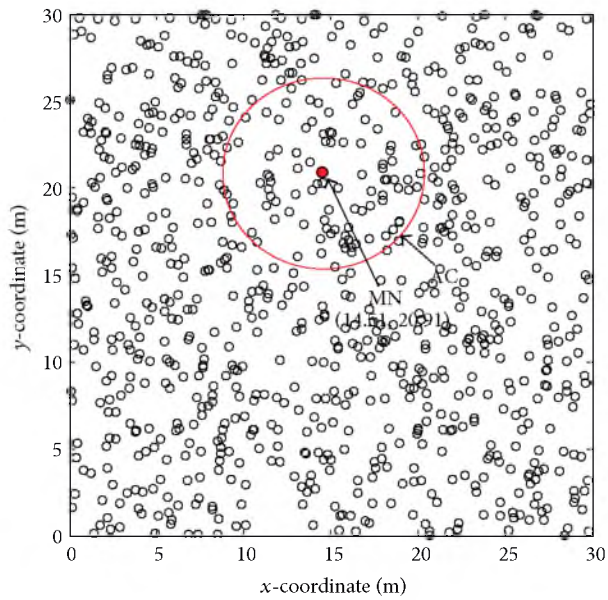

FIGURE 3: Randomly deployed Z nodes with selected MN and AC.

Step 6. Change radius of both r^{UCA} for UCA and r^{CCB} for CCB, with both depending on the desired size of beamwidth.

Step 6(a). Return to Step 1 for different virtual circles.

Step 6(b). Compare the radiation beampattern performance results for different r values.

Step 7. Select the best solution.

The final solution from the proposed CCB is to select the active nodes to perform CB. The intelligent feature in this proposed algorithm is how the algorithm managed to select the best team of active nodes to accomplish CB with user desired requirements. Examples of such requirements are the desired radiation beampattern with minimum SLL and expected size of FNBW. Results are then validated with UCA [12] and circular sensor node array (CSA) as evidence of the effectiveness. Active nodes of CSA are selected based on the UCA, which has the nearest location to nodes of UCA. In CSA optimization setup phase, Step 2 of establishing HLPSO is not included because the distance between nodes d_{sn} of CSA are directly from the distance between nodes of UCA.

4. Results and Analysis

The computed optimization results in radiation beampatterns are analyzed in different cases of N-node CCB with different objectives. The validation performances are demonstrated between CCB and corresponding results obtained from the CSA and conventional UCA [12].

Figure 3 illustrates the simulation scenario for 8-node CCB in MATLAB environment. It shows the random deployment of Z nodes inside the area of interest, that is, Λ, with selected MN. Initially, Z nodes are in a sleep mode. The red

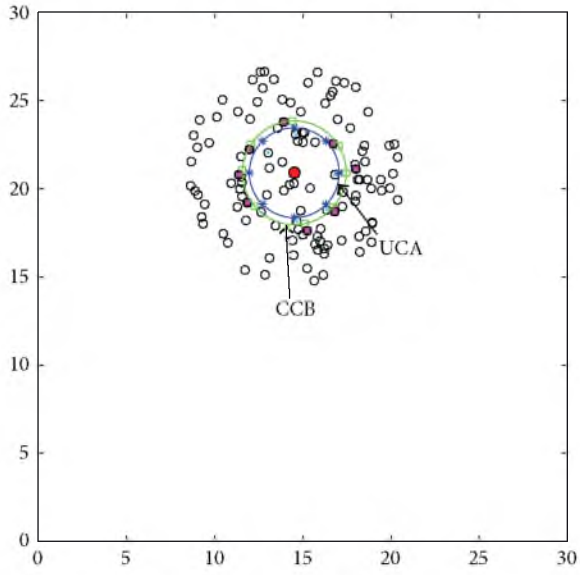

FIGURE 4: Virtual circles (a) blue depicts UCA and (b) green depicts CCB, and nodes (c) blue stars depict A_n, (d) green squares depict B_n, (e) blue circles depict R_n, and (f) square magentas depict M_n.

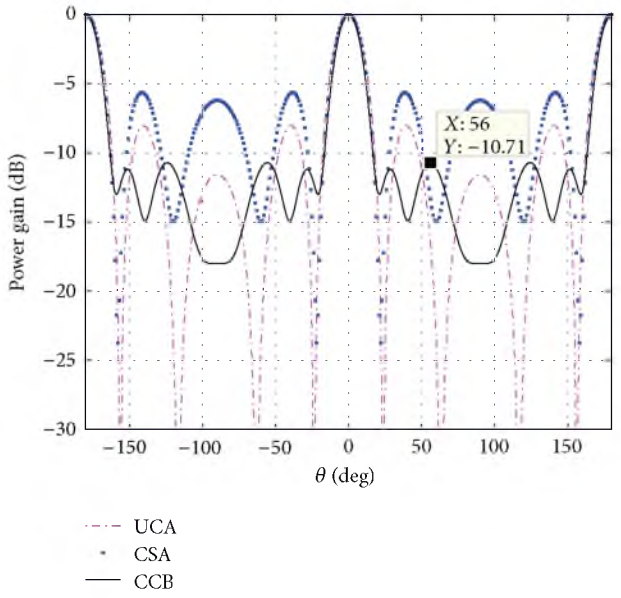

FIGURE 5: Radiation beampattern of 8-node CCB with SLL minimization.

circle marks the AC area, that is, X, with MN at the center of the AC. Figure 4 only highlights the nodes inside the AC. These Z_S nodes are in an idle mode, waiting for any instructions from MN or the center controller. Green circle is a virtual circle with r^{CCB}. Green squares denote coordinates for HLPSO-based nodes, $B_n(x_n^B, y_n^B)$, while square magentas denote CCB active nodes, $M_n(x_n^M, y_n^M)$. The CSA active nodes, R_n, are represented by light blue circles.

Table 3 lists the x- and y-coordinates for B_n and M_n for $n = 1, 2, \ldots, 8$ nodes. The Euclidean distance errors

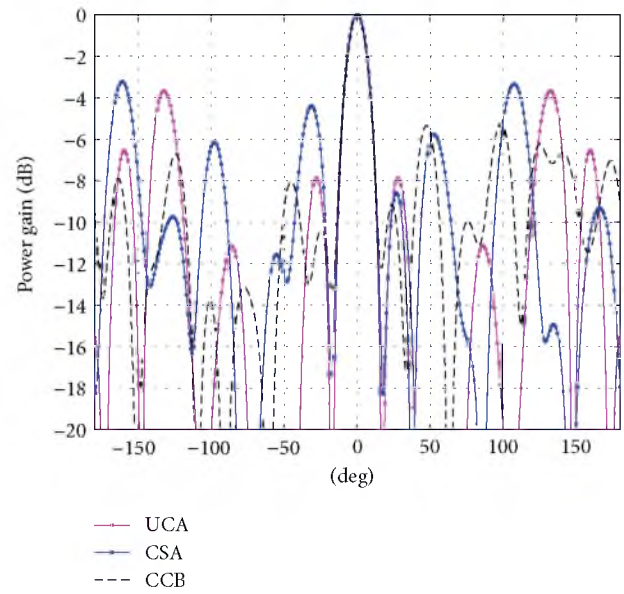

FIGURE 6: Radiation beampattern of 8-node CCB with SLL minimization.

ε_n between HLPSO-based nodes B_n and the proposed CCB active nodes M_n are also demonstrated in the same table. The sum average for all distances for 8-node CCB is calculated as 0.4021.

4.1. Sidelobe Level (SLL) Suppression. In the proposed CCB, SLL can be successfully suppressed to increase the received power at the receivers and to avoid interference from other interrupting access points or clusters or prevent these access points or clusters from recovering the transmitted signal. Figure 5 demonstrates the computed normalized gain for 8-node CCB at x-z plane ($\phi = 0^\circ$). It is observed that, for 360° radiation beampattern, the main beam gain exists at two different angles, that is, 0° and 180°. The maximum SLL obtained is low which is only −10.71 dB, while the maximum SLLs of UCA and CSA are approximately −8.03 dB and −5.63 dB, respectively.

The optimization then considers a circular array with FNBW of 38° with the main beam angle pointing towards $\theta_0 = 0^\circ$. Figure 6 shows the computed radiation beampatterns for y-z plane ($\phi = 90^\circ$), magenta curve for UCA with fixed spacing of $\lambda/2$ between elements, and blue curve for CSA, whereas black curve was proposed for CCB by using HLPSO. It can be clearly observed that the SLL suppression of CCB is generally better than that obtained from both UCA and CSA. All the minor lobes have been successfully minimized with the highest peak SLL to be approximately −5.20 dB compared to the maximum SLL of UCA and CSA of −3.66 dB and −3.21 dB, respectively. The two high lobes at −132° and 132° which exist in UCA have been greatly suppressed in this newly proposed CCB by considerable amount of 4 dB and 2 dB, respectively. At y-z plane, only one main beam exists in CCB for 360° radiation beampattern. These showed that the weakness of LSNA [8] which generates two main beams in 360° radiation beampattern is improved with CCB.

Table 3: Coordinates of B_n and M_n with difference Euclidean distances, ε_n.

n	x_n^B	y_n^B	x_n^M	y_n^M	$\varepsilon_n = \sqrt{(x_n^M - x_n^B)^2 + (y_n^M - y_n^B)^2}$
1	17.0	22.4	16.7	22.6	0.3374
2	14.4	23.9	13.9	23.8	0.5204
3	12.0	22.5	12.0	22.2	0.3117
4	11.6	21.1	11.4	20.8	0.3362
5	12.3	19.0	11.9	19.2	0.4503
6	15.1	18.0	15.2	17.6	0.4337
7	16.7	18.9	16.8	18.7	0.2445
8	17.5	20.9	18.0	21.1	0.5828
					$\sum_{n=1}^{8} \varepsilon_n/8 = 0.4021$

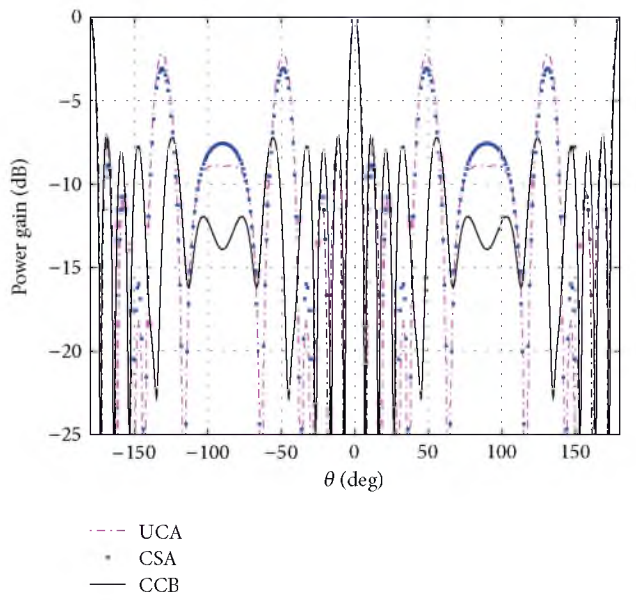

Figure 7: Radiation beampattern of 12-node CCB with SLL minimization.

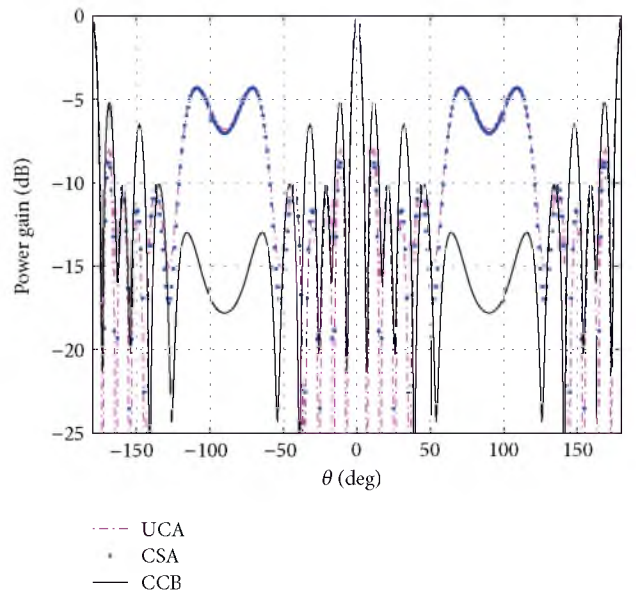

Figure 8: Radiation beampattern of 16-node CCB with SLL minimization.

The next case considers 12-node CCB. It demonstrates the different effects on the radiation beampattern performance with different arrangements of the node location. It can be seen from Figure 7 that the conventional UCA exhibits relatively high SLL at −131°, −49°, 49°, and 131°, which is similar to CSA. The maximum SLL of CCB shows degradation, that is, decrease of 5.02 dB, compared to the maximum SLL of UCA (i.e., −2.19 dB at 49°).

16-node CCB is then considered. It can be observed from Figure 8 that the highest peak SLL of approximately −4.32 dB exists at −109°, −71°, 71°, and 109° for both UCA and CSA. However, CCB managed to greatly minimize the SLL until −14.30 dB at the respective angles. As the number of CB active nodes increases, it not only can increase the gain but also narrows the FNBW as desired. In this case of 16-node ICSA, the FNBW is only 14°.

Three cases are analyzed with different numbers of CCB nodes as shown in Table 4. From the results, it is noted that this newly proposed CCB can overcome the undesired increment of the SLLs in UCA and CSA by intelligently optimizing the participating CB active nodes.

4.2. Controllable First Null Beamwidth (FNBW). An advantage of CCB over UCA and CSA is that the CCB has the capability to adjust the desired amount of FNBW. It is essential to control FNBW in order to decrease the energy consumption. The size of FNBW is needed to be narrower for data transmission to focus the radiation to the attempted destination. In contrast, the size for FNBW is needed to be wider for direction-finding applications.

It reveals the different effects on the size of FNBW performance with the different arrangements of the node location. The radiation patterns of 8-node CCB are plotted in Figure 9. It illustrates a smaller radius of CCB with r = 1.0312, resulting in a wider FNBW of approximately 64° compared to Figure 10 with r = 4.098. It can be seen that the 8-node CCB intelligently accomplishes any desired size of FNBW, either wider or narrower, by optimizing the active

Table 4: Percentage improvement of SLL performance for CCB in different cases.

Case	N	N-node CCB		N-node CSA		N-element UCA		Improvement (%)
		SLL (dB)	FNBW (°)	SLL (dB)	FNBW (°)	SLL (dB)	FNBW (°)	
1	8	−5.2	38	−3.21	38	−3.66	38	61.99
	8	−10.71	46	−5.63	46	−8.03	46	90.23
2	12	−7.04	16	−3.07	16	−2.19	16	129.32
3	16	−14.03	14	−4.32	14	−4.32	14	224.77

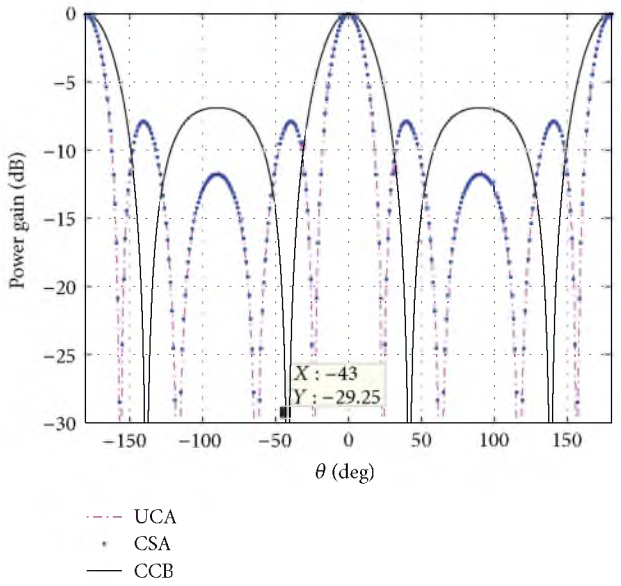

Figure 9: Radiation beampattern of 8-node CCB with wider FNBW.

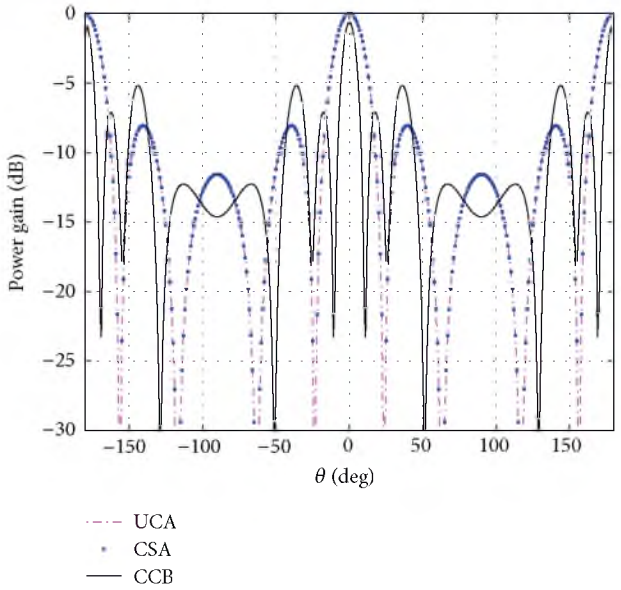

Figure 10: Radiation beampattern of 8-node CCB with narrow FNBW.

CB nodes selection. Both CSA and UCA exemplify a similar performance with $r = 1.9098$. The trade-off performance between SLL and FNBW is obviously illustrated. All the minor SLLs have increased throughout the elevation angles. The SLL increases with adaptive FNBW, both CCB and FNBW of 86° and 22°, generate a higher SLL compared to UCA and CSA.

Next case considers 12-node CCB with $r = 5.9761$ to optimize the size of FNBW The radiation patterns are depicted in Figure 11. It is observed that the FNBW of the optimized 12-node CCB is wider (i.e., 44°) than that of 12-node CSA (i.e., 30°). Additionally, all the minor SLLs have decreased throughout the elevation angles at approximately only −11.51 dB. The subsequent array considered is also a 12-node CCB but with smaller radius of $r = 1.6932$. It shows a larger FNBW (i.e., 50°) as compared to CSA (i.e., 16°) as shown in Figure 12.

It can be observed that a good performance of radiation pattern is obtained from CCB as compared to the previous CSA. It is also shown that different radii contribute to different performances of CCB. In addition, it is noted that the 12-node CCB with FNBW of 50° maintains low SLL throughout the angles that is less than −7.483 dB. Therefore, it is proven that, by implementing the objective function together with CCB, the desired FNBW

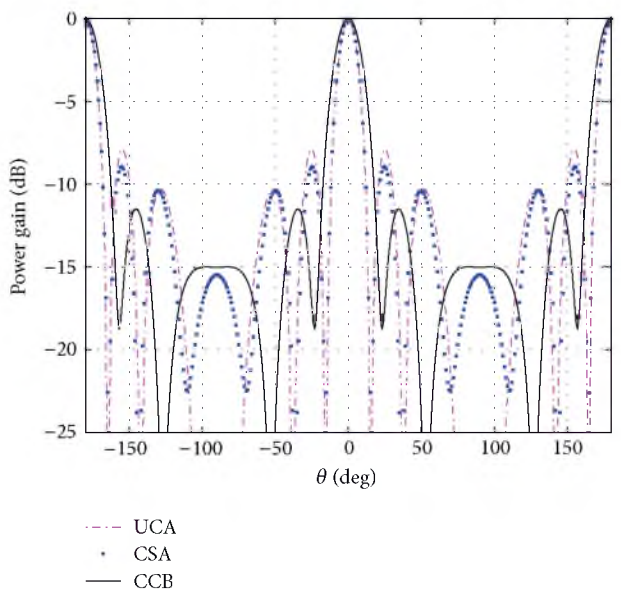

Figure 11: Radiation beampattern of 12-node CCB with narrow FNBW.

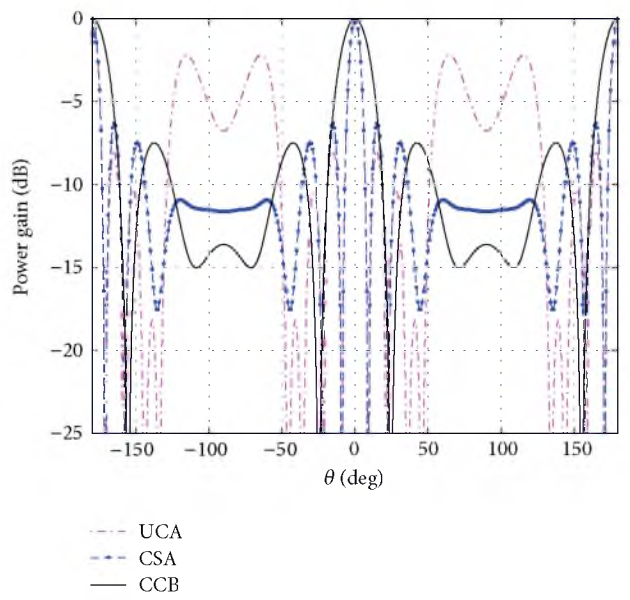

Figure 12: Radiation beampattern of 12-node CCB with wide FNBW.

can be controlled that simultaneously improved the SLL suppression.

5. Conclusion

The problem of array beamforming is the presence of error beampattern caused by random sensor position errors. The proposed CCB can effectively improve reliability, capacity, and coverage by intelligently adjusting the shape of the beam patterns under different constraints, either by suppressing the SLL or managing the size of FNBW as per desired usage. The proposed CCB has the ability to select the active CB nodes and dynamically control the radiation beampattern to enhance the reception while minimizing the interferences using the proposed HLPSO-based CCB algorithms. The radiation beampattern expression of the proposed CCB is obtained, and it is further proved. Different properties of the radiation beampattern have been successfully analyzed and proven.

Acknowledgments

The work is supported by Universiti Teknologi Malaysia and Ministry of Education Malaysia, RUG vote PY/2012/01578 and FRGS vote 4F039.

References

[1] J. Feng, Y. Nimmagadda, Y. H. Lu, B. Jung, D. Peroulis, and Y. C. Hu, "Analysis of energy consumption on data sharing in beamforming for wireless sensor networks," in *Proceedings of the 19th International Conference on Computer Communications and Networks (ICCCN '10)*, pp. 1–6, August 2010.

[2] K. Yao, R. E. Hudson, C. W. Reed, D. Chen, and F. Lorenzelli, "Blind beamforming on a randomly distributed sensor array system," *IEEE Journal on Selected Areas in Communications*, vol. 16, no. 8, pp. 1555–1566, 1998.

[3] M. F. A. Ahmed and S. A. Vorobyov, "Beampattern random behavior in wireless sensor networks with Gaussian distributed sensor nodes," in *Proceedings of the IEEE Canadian Conference on Electrical and Computer Engineering (CCECE '08)*, pp. 257–260, May 2008.

[4] Z. Han and H. V. Poor, "Lifetime improvement of wireless sensor networks by collaborative beamforming and cooperative transmission," in *Proceedings of the IEEE International Conference on Communications (ICC' 07)*, pp. 3954–3958, June 2007.

[5] M. F. A. Ahmed and S. A. Vorobyov, "Node selection for sidelobe control in collaborative beamforming for wireless sensor networks," in *Proceedings of the IEEE 10th Workshop on Signal Processing Advances in Wireless Communications (SPAWC '09)*, pp. 519–523, June 2009.

[6] H. Ochiai, P. Mitran, H. V. Poor, and V. Tarokh, "Collaborative beamforming for distributed wireless ad hoc sensor networks," *IEEE Transactions on Signal Processing*, vol. 53, no. 11, pp. 4110–4124, 2005.

[7] M. F. A. Ahmed and S. A. Vorobyov, "Sidelobe control in collaborative beamforming via node selection," *IEEE Transactions on Signal Processing*, vol. 58, no. 12, pp. 6168–6180, 2010.

[8] N. N. N. A. Malik, M. Esa, S. K. S. Yusof, and S. A. Hamzah, "Optimization of adaptive linear sensor node array in wireless sensor network," in *Proceedings of the Asia-Pacific Microwave Conference (APMC '10)*, pp. 2336–2339, Singapore, December 2009.

[9] N. N. N. A. Malik, M. Esa, S. K. S. Yusof, and S. A. Hamzah, "Optimization of linear sensor node array for wireless sensor networks using Particle Swarm Optimization," in *Proceedings of the Asia-Pacific Microwave Conference (APMC '10)*, pp. 1316–1319, December 2010.

[10] P. Vincent, M. Tummala, and J. McEachen, "A new method for distributing power usage across a sensor network," *Ad Hoc Networks*, vol. 6, no. 8, pp. 1258–1280, 2008.

[11] M. Batson, J. McEachen, and M. Tummala, "Enhanced collection methodology for distributed wireless antenna systems," in *Proceedings of the IEEE International Conference on System of Systems Engineering (SOSE '07)*, April 2007.

[12] C. A. Balanis, *Antenna Theory: Analysis and Design*, Wiley, New York, NY, USA, 3rd edition, 2005.

[13] J. Kennedy and R. Eberhart, "Particle swarm optimization," in *Proceedings of the 1995 IEEE International Conference on Neural Networks*, pp. 1942–1948, December 1995.

[14] Z. Zaharis, D. Kampitaki, A. Papastergiou, A. Hatzigaidas, P. Lazaridis, and M. Spasos, "Optimal design of a linear antenna array using particle swarm optimization," in *Proceedings of the 5th WSEAS International Conference on Data Networks, Communications and Computers*, pp. 69–74, Bucharest, Romania, October 2006.